Space Sci Rev (2008) 141: 35–59
DOI 10.1007/s11214-008-9393-5

THEMIS Science Objectives and Mission Phases

D.G. Sibeck · V. Angelopoulos

Received: 30 March 2008 / Accepted: 2 June 2008 / Published online: 20 June 2008

Abstract The five THEMIS spacecraft and a dedicated ground-based observatory array will pinpoint when and where substorms occur, thereby providing the observations needed to identify the processes that cause substorms to suddenly release solar wind energy stored within the Earth's magnetotail. The primary science which drove the mission design enables unprecedented observations relevant to magnetospheric research areas ranging from the foreshock to the Earth's radiation belts. This paper describes how THEMIS will reach closure on its baseline scientific objectives as a function of mission phase.

Keywords THEMIS · Magnetosphere · Substorms · Radiation belts · Magnetopause

1 Introduction

THEMIS (Time History of Events and Macroscale Interactions during Substorms) is NASA's fifth MIDEX mission, following in the successful footsteps of FUSE, IMAGE, WMAP, and Swift. THEMIS will provide the multipoint and multi-instrument observations needed to determine why the transfer of solar wind energy to the Earth's inner magnetosphere and ionosphere generally occurs via geomagnetic substorms. As the building blocks of solar wind-magnetosphere interaction, substorms encompass a wide array of magnetospheric phenomena including sudden reconfigurations of the nightside magnetospheric magnetic field, jetting plasmas, injections of energetic ions and electrons into the Earth's radiation belts, field-aligned beams of energetic particles and currents directed from the magnetotail to the ionosphere, auroral displays, and associated disturbances in surface magnetic fields.

Of the many proposed substorm models, two have become widely accepted on the basis of their ability to explain the full panoply of observed phenomena. The current disruption

D.G. Sibeck (✉)
Code 674, GSFC/NASA, Greenbelt, MD 20771, USA
e-mail: david.g.sibeck@nasa.gov

V. Angelopoulos
IGPP, UCLA, Los Angeles, CA 90095, USA
e-mail: vassilis@ucla.edu

model predicts that substorms begin with a disruption of the cross-tail current about 8 to 10 Earth radii (R_E) from Earth, while the reconnection model predicts that substorms begin with the onset of reconnection in the current sheet some 20 to 30 R_E from Earth. Despite their strikingly different predictions concerning when and where substorms begin, the lack of coordinated high time resolution multipoint and multi-instrument observations has precluded efforts to discriminate between these two (and other) models.

NASA's THEMIS mission, managed by the University of California at Berkeley, will enable researchers to pinpoint when and where substorm onsets occur. The identical instruments on each of the five THEMIS spacecraft were selected to identify both substorm signatures and the physical processes that trigger them, while the orbits of the THEMIS spacecraft were chosen to bound proposed locations where substorms begin. A dedicated array of ground observatories located throughout Canada, Alaska, and the northern regions of the contiguous United States supplies the global observations needed to place the multipoint, but isolated, spacecraft observations in context.

While in the magnetotail, the THEMIS spacecraft will also provide important observations concerning the consequences of magnetospheric substorms, including the generation of field-aligned currents by vortical plasma flows and pressure gradients, and the coupling of substorm disturbances to local instabilities responsible for geomagnetic pulsations and ballooning modes. THEMIS observations of the Earth's radiation belts will be used to determine the means by which ions and electrons are energized, transported, and lost. Finally, the THEMIS spacecraft will spend many months on the dayside, where their observations will enable researchers to discriminate between various modes of steady and transient solar wind-magnetosphere interaction.

Angelopoulos (2008) provides a mission overview, summarizing the overall scientific objectives, orbits, instrumentation, mission and science operations that are expanded upon in individual papers in this compendium. In this paper we address how the above mission elements will enable the THEMIS team to reach closure on its science objectives as function of mission phase. In terms of organization, Sect. 2 summarizes the THEMIS science objectives and Sect. 3 describes the THEMIS mission elements. Sections 4 to 6 outline THEMIS science objectives as a function of mission phase: the nightside magnetotail phases, the dayside phases and ongoing observations throughout the mission life within the Earth's radiation belts. Section 7 presents conclusions.

2 THEMIS Science Objectives

2.1 Substorms

Substorms represent a fundamental mode of solar wind-magnetosphere interaction, an interaction that transfers energy from the solar wind and deposits it in the Earth's ionosphere, atmosphere, and radiation belts (Akasofu 1977). Substorms follow a clear and repeatable cycle. During the growth phase, southward turnings of the interplanetary magnetic field (IMF) initiate reconnection on the dayside magnetopause. The removal of newly reconnected magnetic flux reduces dayside magnetospheric magnetic field strengths and pressures, while the addition of the same flux to the nightside magnetosphere enhances magnetotail magnetic field strengths and pressures. As a result, the dayside magnetopause moves inward, the magnetotail magnetopause flares outward, the plasma sheet thins, and cross-tail currents increase to accommodate a stretched, tail-like, magnetic field configuration. The region of open magnetic field lines over the polar caps expands and quiet time aurorae move equatorward.

Just prior to substorm onset, strong (10's nA m^{-2}) cross-tail currents, generated primarily by duskward anisotropies of 2 to 10 keV ions, appear in the near-Earth ($\sim$10 R_E from Earth) magnetotail (Lui 1996). Just after substorm onset, these cross-tail currents are diverted to flow through the ionosphere, and stretched magnetotail magnetic field lines suddenly snap back towards more dipolar configurations. Plasma flows rapidly both sunward and anti-sunward away from reconnection sites in the plasma sheet typically some 20 or 30 R_E from Earth. Beams of energized particles flow sunward along the boundaries of the plasma sheet, reflect upon reaching near-Earth mirror points and flow back into the plasma sheet at slightly lower latitudes. Particles that do not reflect precipitate into the ionosphere, brightening pre-existing auroral arcs. The auroral brightening expands rapidly poleward into the polar cap as reconnection converts open-lobe magnetic field lines into closed plasma sheet magnetic field lines. The collapse of nightside magnetic field lines into more dipolar configurations injects energetic particles into near-Earth geospace.

Two models seek to explain the sequence of events that occur during geomagnetic substorms. The current-disruption or near-Earth initiation model, shown in the top panel of Fig. 1, predicts that the strong currents that appear within the near-Earth magnetotail at substorm onset trigger instabilities that result in the collapse of the stretched magnetotail magnetic field to a more dipolar orientation, current diversion to and through the ionosphere, the injection of a heated plasma into the inner magnetosphere, and the launching of a fast rarefaction wave that propagates down the magnetotail and initiates reconnection at greater distances (Lui 1996). Advocates interpret (1) the explosive growth and then collapse of cross-tail currents in the near-Earth magnetotail at substorm onset, (2) the initial brightening of the most equatorward pre-existing auroral arc, which maps to locations deep within the magnetosphere, (3) the initial appearance of enhanced particle fluxes earthward of spacecraft located in the near-Earth magnetotail, and (4) the initial appearance of enhanced cosmic noise absorption caused by precipitating energetic electrons at the equatorward edge of the auroral oval as evidence for the current disruption model paradigm.

By contrast, the reconnection or mid-tail initiation model shown in the bottom panel of Fig. 1 invokes a current-driven instability that triggers reconnection some $\sim$25 R_E down the magnetotail (Hones 1976; Baker et al. 1996; Shiokawa et al. 1997). Reconnection launches fast, often bursty, flows that transport plasma and magnetic flux sunward towards the inner magnetosphere. The inner magnetosphere poses an obstacle that brakes and deflects these flows and converts their kinetic energy to thermal energies and enhanced magnetic field strengths in a dipolar configuration. Precipitating particles and field-aligned currents associated with the flow braking generate aurorae and magnetic field disturbances. Advocates interpret (1) the tendency of sunward flows to be associated with northward magnetic fields and anti-sunward flows to be associated with southward magnetic fields, (2) the appearance of magnetic field perturbations expected for Hall current effects, and (3) the anti-sunward motion of plasmoid bubbles released at substorm onset as evidence for the reconnection model.

Accurate, multipoint measurements that pinpoint the location(s) where substorms begin and the timing of the phenomena that follow can distinguish between these two models (e.g. Baker et al. 2002). In the current disruption model, the sequence should be: (1) current disruption some 8 to 10 R_E from Earth, (2) auroral breakup, and (3) magnetic reconnection at greater distances down the magnetotail. By contrast, in the reconnection model, the sequence of events should be: (1) reconnection some 25 R_E from Earth, (2) current disruption in the near-Earth tail, and (3) auroral breakup. It is important to characterize substorms as a function of solar wind conditions, not least because abrupt northward IMF turnings or solar wind dynamic pressure increases may trigger current disruption or magnetic reconnection (e.g. McPherron et al. 1986).

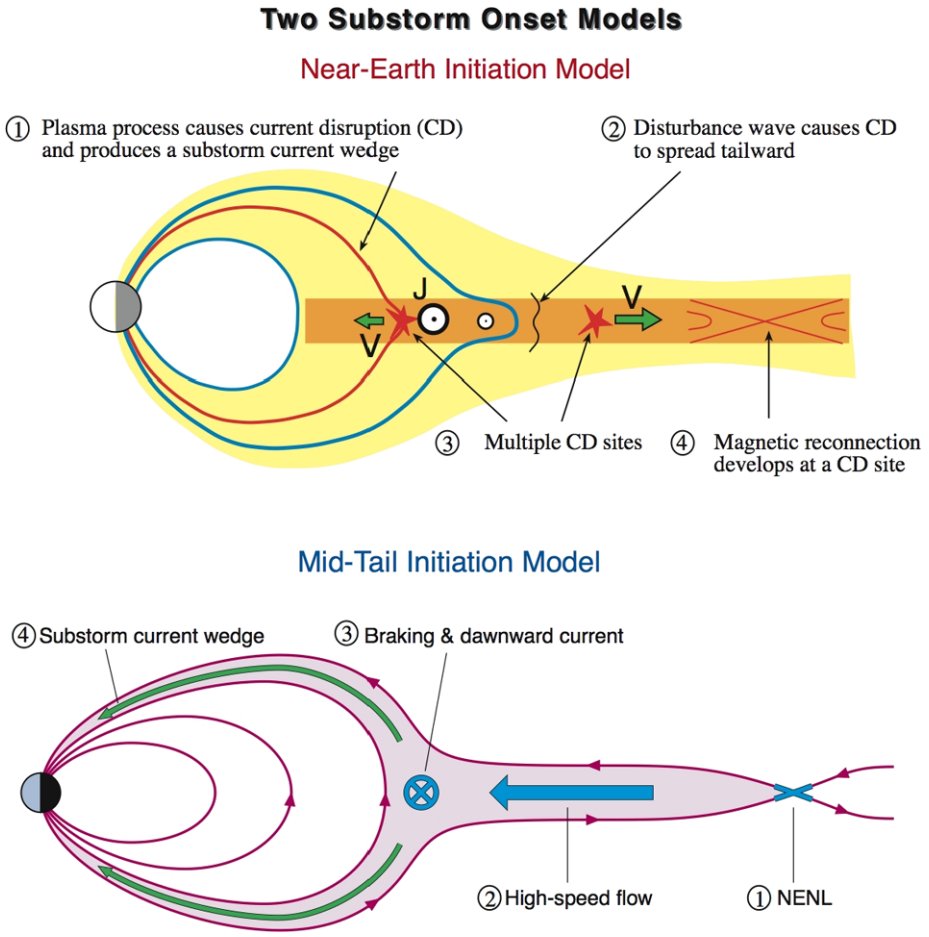

Fig. 1 Current disruption (near-Earth initiation) and reconnection (mid-tail initiation) models for geomagnetic substorms. In the current disruption model, a sudden disruption of the cross-tail current in the near-Earth magnetotail launches a tailward propagating rarefaction wave that initiates reconnection further down the magnetotail. The disrupted current flows into the ionosphere along magnetic field lines and the aurora brightens. In the reconnection model, reconnection in the mid-magnetotail launches sunward propagating flows and a fast mode compressional wave that cause magnetic flux to pile up in the near-Earth magnetotail. Flow shears or flow breaking launch currents that flow along magnetic field lines into the ionosphere and the aurora brightens

In the process of determining the mechanism(s) that drive geomagnetic substorms, THEMIS will also address both fundamental plasma physics questions and space weather forecasting needs. The cross-scale coupling and particle energization processes that occur during substorms may be ubiquitous throughout the plasma universe. Microphysical instabilities at the cross-tail current sheet trigger mesoscale flows within the Earth's magnetotail, which in turn result in macroscale reconfigurations of the entire magnetosphere. Stressed current sheets like those that occur within the Earth's magnetotail can also be found in fusion devices, throughout the heliosphere, at the Sun and other stars, and in other planetary magnetospheres. Consequently, the multipoint THEMIS measurements offer an opportunity

to test conflicting model (and simulation) predictions against in situ observations and apply the knowledge gained to other systems where this is not possible.

The practical impact of THEMIS on space weather forecasting is equally important. For a variety of operational purposes, it is important to predict the occurrence of substorm-generated geomagnetic disturbances and corresponding auroral displays. THEMIS will provide the scientific understanding needed to advance our forecasting capabilities towards the ability to predict substorm onset time, extent, and amplitude.

2.2 Radiation Belts

Despite more than 40 years of study, the processes that generate, transport, and remove energetic particles in the Earth's radiation belts remain unclear. Proposed acceleration and injection mechanisms include direct energization by electric fields associated with large- and small-scale storm-time convective flows into the inner magnetosphere (Khazanov et al. 2004), impulsive energization via substorm-launched inward-propagating injection fronts (Mithaiwala and Horton 2005), radial diffusion and energization by storm-time ULF waves (Loto'aniu et al. 2006) or solar wind dynamic pressure variations (Ukhorskiy et al. 2006); energization by VLF waves followed by pitch angle anisotropization (Horne et al. 2005), impulsive trapping of solar energetic ions during geomagnetic storms (Kress et al. 2005), and prompt acceleration by compressional wave fronts associated with strong interplanetary shocks (Hudson et al. 1995). Proposed loss mechanisms are no less numerous than energization mechanisms. They include pitch angle scattering into the ionosphere via cyclotron and Landau resonant interactions with plasmaspheric hiss, whistler-mode chorus, and EMIC waves, scattering by interaction with the magnetotail current sheet, and magnetopause shadowing (Green et al. 2004; Millan and Thorne 2007).

As illustrated in Fig. 2 (Li et al. 2001), recurrent geomagnetic storms generate dramatic variations in energetic particle fluxes within the inner magnetosphere. THEMIS will supply the multipoint and multi-instrument observations needed to discriminate between the various mechanisms proposed to account for the appearance, transport, and loss of ions and electrons with energies less than 1 MeV. The results obtained by THEMIS will be used to help plan NASA's forthcoming LWS radiation Belt Storm Probe mission, which is dedicated to understanding the processes governing the more energetic (and more hazardous) particles found within the Earth's radiation belts.

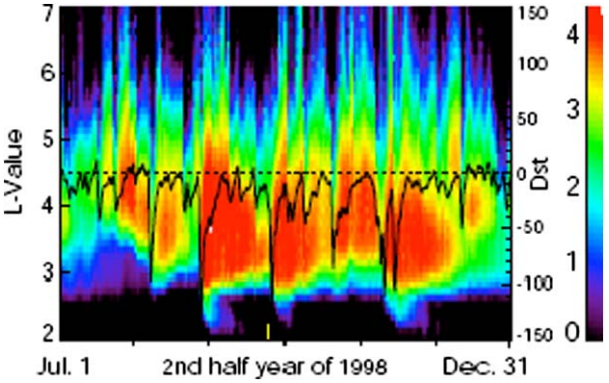

Fig. 2 Daily averaged SAMPEX electron measurements of 2–6 MeV electrons (#/cm^2-s-sr) and Dst index with 1-day window-average for the second half year of 1998 (Li et al. 2001). The *black line* shows the Dst index, a measure of geomagnetic storm activity

2.3 Dayside Interactions

Many aspects of the dayside interaction between the solar wind and magnetosphere remain poorly understood. For example, we do not know when our use of solar wind monitors far upstream or far off the Sun-Earth line to measure the solar wind input into the magnetosphere is valid, because we do not know the scale sizes for solar wind features and understand poorly the processes that modify these features within the Earth's foreshock and magnetosheath. Nevertheless, in recent years it has become apparent that kinetic processes within both these regions can result in drastic, albeit transient, perturbations to the incoming solar wind density, velocity, and magnetic field strength. Figure 3 shows hybrid code model predictions for the distribution of plasma ion densities and temperatures in the vicinity of the dayside bow shock attending the passage of a solar wind tangential discontinuity (Omidi and Sibeck 2007). Kinetic processes result in the development of a hot flow anomaly within the solar wind at the intersection of the discontinuity with the bow shock (Thomsen et al. 1988). The density variations associated with such structures launch the full spectrum of waves when they strike the bow shock and magnetopause. The propagation paths of these waves remain unclear but may provide important information concerning the distribution of plasmas in and around the magnetosphere.

The magnetopause is constantly in motion. The motion may be directly driven by transmitted solar wind and foreshock-generated pressure variations (Farrugia et al. 1989), result from the Kelvin-Helmholtz instability (Otto and Fairfield 2000), or be triggered by bursts of reconnection (Song et al. 1988). As illustrated in Fig. 4, bursts of reconnection generate twisted ropes of interconnected magnetospheric and magnetosheath magnetic field lines (Russell and Elphic 1978). Discriminating between these possibilities for any individual event requires simultaneous solar wind, magnetosheath, and magnetopause observations, while statistical studies designed to determine the significance of each proposed mechanism require surveys of event occurrence patterns, dimensions, growth, and decay as a function of solar wind conditions. THEMIS will provide the observations needed to address these dayside science topics.

3 Mission Elements

The five spin-stabilized THEMIS spacecraft have 3 s spin periods and carry identical high-heritage instruments. The triaxial fluxgate magnetometer (FGM) measures DC and low-frequency perturbations of the magnetic field (Auster et al. 2008), times the propagation of waves and plasma structures between spacecraft, and provides information concerning currents flowing between two or more probes. Accuracies, stabilities, and interference from spacecraft systems are 0.3 nT or better. A pair of back-to-back top hat hemispherical electrostatic analyzers (ESA) measures the distribution functions of thermal ions (0.005 to 25 keV) and electrons (0.005 to 30 keV) over 4π-str to determine accurate 3 s time resolution plasma moments and instantaneous gradients in these parameters between probes (Carlson et al. 2008; McFadden et al. 2008).

Solid-state telescopes (SST), each comprising two sensors, measure the superthermal (0.02–1 MeV) part of the ion and electron distributions over 3π str (Larson et al. 2008). Mechanical attenuators diminish the geometric factor within the radiation belts (radial distances from Earth below 8 R_E) by a factor of $\sim$100, thereby limiting damage to the silicon detectors from intense fluxes of low energy ions. The telescopes will be used to remotely sense the current disruption region and time the arrival of particles energized by reconnection.

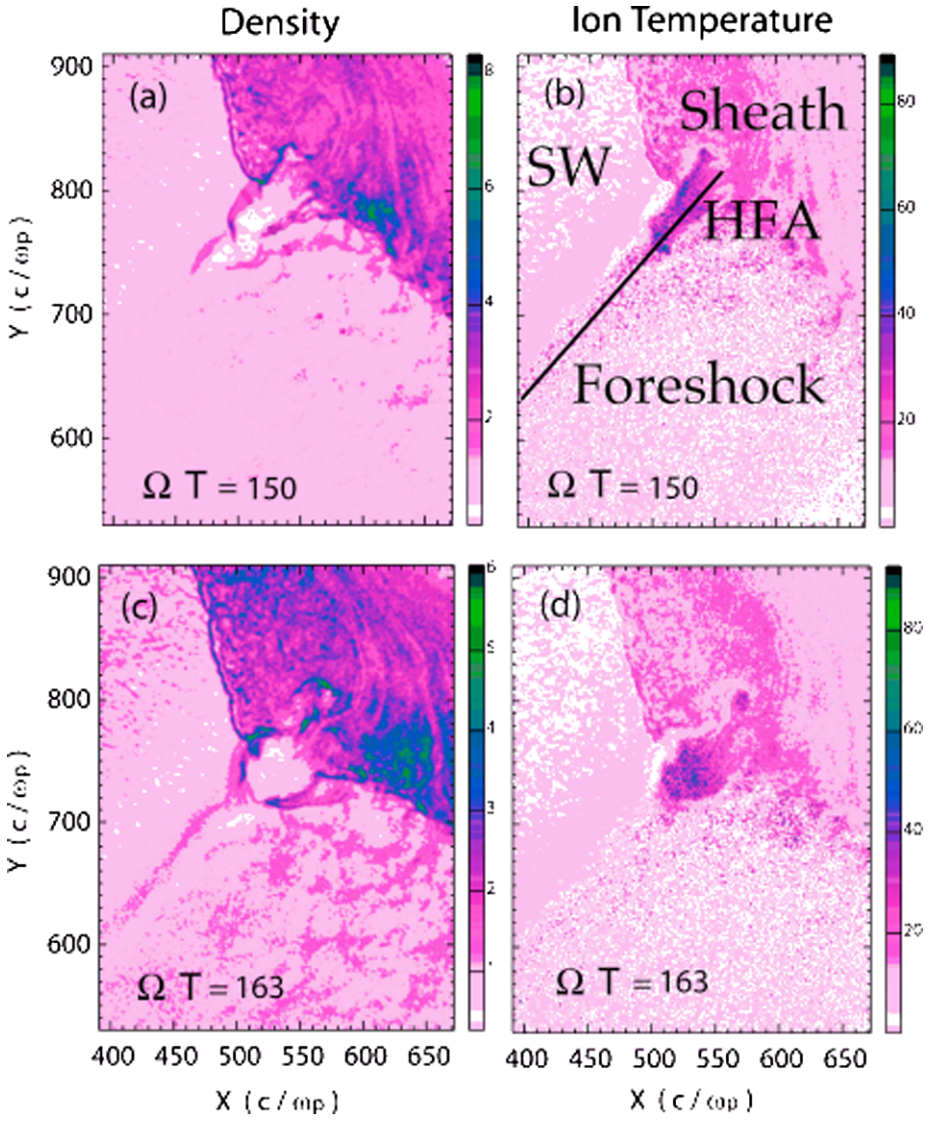

Fig. 3 Hybrid code simulation results for the formation of a HFA at the intersection of an interplanetary discontinuity with the Earth's bow shock (Omidi and Sibeck 2007). The panels on the *left* show densities, while those on the *right* show ion temperatures. Two stages in the development of the HFA are shown, at $\Omega T = 150$ and 163, where Ω is the ion gyrofrequency. The *solid black line* in the *upper right* panel indicates the location of the IMF discontinuity

Search coil magnetometers (SCM) extend the measurements of the FGM from 0.1 Hz to frequencies of 4 kHz (Roux et al. 2008). Sensitivities of $0.8 pT/\sqrt{\text{Hz}}$ at 10 Hz and $0.02 pT/\sqrt{\text{Hz}}$ at 1 kHz suffice to measure the waves that accompany cross-tail current disruptions some 8 R_{E} from Earth. Periodic calibration using the discrete signals generated by coils ensures accurate measurements. Each electric field instrument (EFI) employs two pairs of spherical sensors on 20 and 25 m deployable cables and a pair of axial tubular sensors

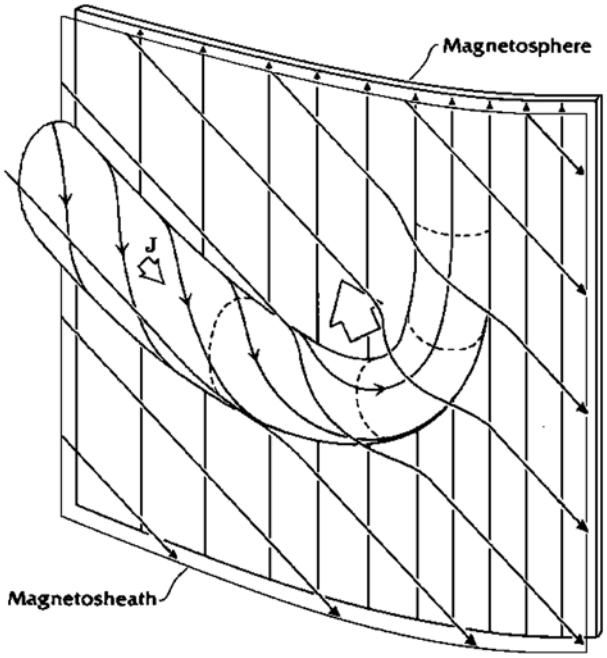

Fig. 4 Flux transfer events (FTEs) are twisted ropes of interconnected magnetospheric and magnetosheath magnetic field lines (Russell and Elphic 1978)

on 3.0 m whip booms to make three-dimensional electric field measurements at frequencies up to 300 kHz (Bonnell et al. 2008). EFI observations can be used to determine the ambient density, plasma convection velocities, wave modes, and the Poynting flux.

The Instrument Data Processing Unit (IDPU) handles on-board particle data collection and moment computations, processes field data and performs spin fit computations, executes memory storage and compression, and communicates with the spacecraft computer for data transmission. Both independent and inter-spacecraft calibrations during quiet time conjunctions ensure that errors in moment calculations do not exceed 10%.

Stored or triggered commands cause the instruments on the spacecraft to operate in one of four modes: slow or fast survey, particle or wave burst. Throughout most of their orbits, the spacecraft operate in slow survey mode, returning magnetic field vectors, plasma moments, and other parameters with 3 s time resolution. Near apogee in the magnetotail and in regions of interest like the dayside magnetopause, stored commands trigger the instruments to operate in fast survey mode. In fast survey mode, FGM samples the magnetic field 16 times per spin, SCM and EFI sample 32 times per spin, and SST and ESA provide observations with greater spatial resolution. Encounters with the bow shock, magnetopause, bursty bulks flows within the magnetotail, magnetic field reconfigurations, and other phenomena trigger burst mode operations. In burst mode, FGM can sample the magnetic field at up to 128 Hz, while SCM and EFI can sample at up to 4096 Hz.

A dedicated dense network of 20 all-sky white light imagers and ground magnetometers (when no pre-existing magnetometer is located nearby) covering the Arctic and mid-latitude regions of North America ensures accurate determination of substorm onset locations to within 0.5 hours of magnetic local time (Mende et al. 2008). The magnetometers have 0.5 s time resolution, while the imagers take snapshots of duration $\sim$1 s each 3 s.

The five THEMIS spacecraft operate in highly elliptical, near-equatorial, orbits that precess about the Earth. At 23:01 UT on February 17, 2007, the spacecraft were launched into

common initial orbits with geocentric apogee at 14.7 R_E and 2100 LT, geocentric perigee at 1.07 R_E, inclination of 16°, and orbital periods of 31 hours. During the coast phase of the mission, from launch until September 2007, apogees precessed through the dusk and dayside magnetosphere. Interspacecraft separations ranged from a few 100 km to 2 R_E along track. This orbit phase was prefixed on the baseline mission design to avoid a mission redesign late in the program after the launch vehicle provider announced a launch delay that caused the mission to slip past its ability to perform tail studies in the winter of 2007. From September 15 to December 15, 2007, the spacecraft were on the dawnside of the Earth's magnetosphere, where their apogees were moved to 31.0, 19.6, 11.8, 11.8 and 9.9 R_E in anticipation of the tail season. The corresponding orbital periods during the first magnetotail phase of the mission from December 15, 2007 to April 15, 2008 were ∼1, 2, and 4 days, enabling the radial alignments of the spacecraft apogees needed to address the baseline substorm science once every 4 days. During this period probe P5 was separated in apogee from P3 and P4 by 2 R_E, resulting in an orbital period that was 4/5 that for P3 and P4. Probe P5 thus participated in a major conjunction once every 5 orbits, or 4 days, but was separated from the other probes by several R_E the rest of the time. This enables a wide range of azimuthal separations, but also provides for 1–3 R_E clustering during major conjunctions along the orbit plane.

Six months after the first tail season, the first dayside observations commence. The orbital configuration remains the same, but the apogee of P5 is reduced to lie only 1 R_E away from those of P3 and 4 to reduce differential precession. Major conjunctions between 4 spacecraft occur once every 4 days, but P5 is tightly clustered with P3/4 only once per 8 days, and therefore scans a large range of azimuthal separations with P3 and 4 the rest of the time. The spacecraft return to the Earth's magnetotail for a second season of substorm observations from December 15, 2008 to April 15, 2009. During this second season, the orbits of the three inner spacecraft will have common apogees of 11.6 R_E, but due to a 5° difference in orbital inclinations, P5 will be separated from P3 and 4 by ∼1 R_E in Z_{GSM} at apogee. The separation is designed to enable researchers to determine the properties of the near-Earth current and plasma sheet. Azimuthal separations of ∼ 1 R_E between P3 and P4 are designed to identify simultaneous current disruptions. Figure 5 illustrates representative four-day-long orbital segments throughout the nominal mission.

4 Science Closure in the Magnetotail

THEMIS will provide the observations needed to discriminate between conflicting models for geomagnetic substorms by determining when, where, and why substorm onset occurs. Every four days the THEMIS spacecraft will line up within the Earth's magnetotail, affording opportunities to conduct timing studies of substorm features as a function of distance down the magnetotail. As illustrated in Fig. 6, spacecraft P1 and P2 will bound the expected location of the reconnection line. Observations of high-speed sunward flows and northward magnetic field orientations at P2, but anti-sunward flows and southward field orientations at P1, will demonstrate the appearance of a reconnection line between the two spacecraft.

THEMIS probes P3–5 lie near the expected location of current disruption within the Earth's magnetotail. These spacecraft will be used to time the changes in plasma and magnetic field configuration that occur in the near-earth magnetotail for comparison with the times determined for reconnection from probe P1 and P2 observations. Timing and remote sensing techniques employing the energetic particles observations will be used to discriminate between sunward-propagating compressional events that begin in the distant

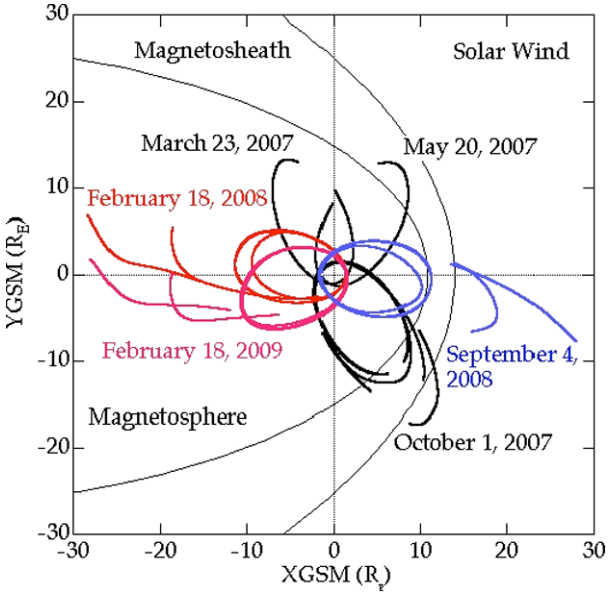

Fig. 5 Day-long intervals of ephemeris at representative stages of the mission. In March and May of 2007, the spacecraft were in nearly-identical orbits with apogee on the duskside of the Earth. By October 2007, apogee separation had begun and the spacecraft were on the dayside of the Earth. In February 2008, the spacecraft apogees will be fully separated and in the Earth's magnetotail. By September 2008, the spacecraft will be on the dayside again. In February 2009, the orbits of the three innermost spacecraft will have similar apogees, but different inclinations

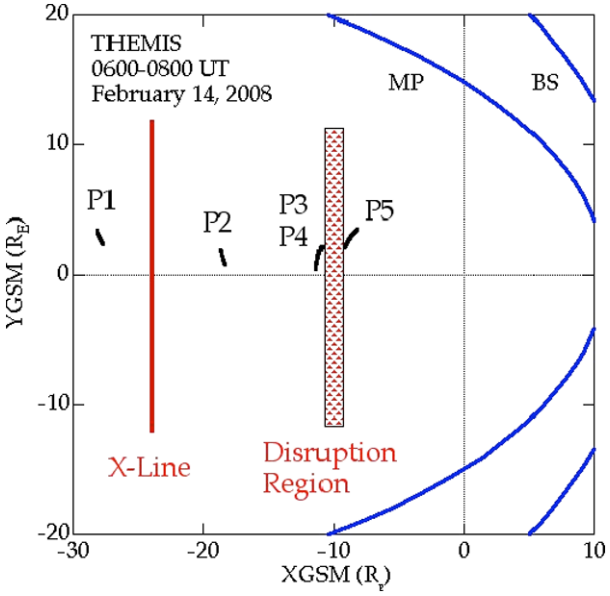

Fig. 6 The trajectories of the THEMIS spacecraft from 06:00 to 08:00 UT on February 14, 2008. Spacecraft P1 and P2 bound the reconnection line. Spacecraft P5 and closely-spaced spacecraft P3 and P4 bound the current disruption region

magnetotail and anti-sunward-propagating rarefaction events that begin in the near-Earth magnetotail.

4.1 Time History of Events

To distinguish between proposed models for substorms, THEMIS must time their onset. Based on current orbit predictions (Frey et al. 2008), the THEMIS probes will accumulate more than 250 h/year of tail-aligned conjunctions (no spacecraft separated by more

than 2 R_E in the cross-tail or Y-direction from P1). With alignments lasting ∼12 hours, and substorms recurring every ∼3 hours, each alignment should result in 3–4 substorms for a mission total of ∼80 substorms. At least a dozen of these should be observed from the pre-midnight substorm onset meridian. With these data THEMIS will be able to delineate the time history of the events that comprise the substorm process. THEMIS will rely upon WIND, ACE and, on occasion, Cluster and Stereo to define the external solar wind conditions and distinguish between the different paths to substorm onset. Specific timing techniques include:

Current disruption (CD) onset determination At speeds of 200 km s^{-1}, a current disruption onset 1 R_E away expands over the THEMIS probes within 30 s. THEMIS probes P3 and 4 will employ remote sensing (finite gyroradius) techniques to obtain timing information from energetic ion observations (Lui et al. 1988; Ohtani 1998) applied to energetic ions. This method provides boundary expansion speeds to within 10 km s^{-1} and directions measured to a fraction of the angular resolution of the ion detector (Daly et al. 1984; Kettmann and Daly 1988). Onset times will be determined from the expansion velocities on the two nearby probes to within the 3 s probe time resolution, ensuring current disruption timing to within 10 s or better.

Reconnection (Rx) onset determination THEMIS will time the onset of reconnection by monitoring the arrival times of field-aligned energetic particles from the reconnection site at its two outer probes, located within 5 R_E from the nominal site of reconnection some 25 R_E from Earth. Ancillary timing information will be obtained from measured flow speeds and local observations of electrons, waves, and the MHD pulse from the reconnection process (Sarris et al. 1976; Petrukovich et al. 1998). THEMIS will provide reconnection onset timing to within 10 s or better.

Auroral breakup onset determination Although mid-latitude ground magnetometers have long been used to identify global Pi2 pulsations and thereby determine the time of substorm onset, much more accurate timing can be obtained from high-latitude imagers and ground magnetometers (Olson 1999; Liou et al. 2000). The network of white light all sky imager and ground magnetometer stations in Alaska, Canada and the US will ensure accurate determination of onset to within 0.5° in magnetic local time (Mende et al. 2008). Cloudy skies or moonlight sometimes obscure the images. At these times, PiB (1–40 s period, 3 s nominal) pulsations (Heacock 1967), which are good substorm indicators (Troitskaya 1961; Bösinger et al. 1981), will determine onset time to within a few seconds. Substorm current wedge modeling from a dense North American network of auroral and mid-latitude magnetometer stations provides determination of the substorm meridian to within 5° or better (still fulfilling the science goal of 6°). Such modeling is routinely performed using data from the existing network of mid-latitude stations (Clauer and McPherron 1974; Kubyshkina 1999) and has been validated using global imaging (Sergeev et al. 1996). In short, THEMIS's ground network of all sky imager and ground magnetometer stations has the density and time resolution to detect auroral breakup onset meridian and onset time nominally within δMLT $< 0.5°$, $\delta t < 10$ s. Figure 7 combines information from the THEMIS arrays of all-sky cameras and ground magnetometers to depict an instant (06:19:36 UT on December 23, 2006) and a location (marked by the white box) when the aurora brightened and there was a strong shear in the magnetic field perturbations.

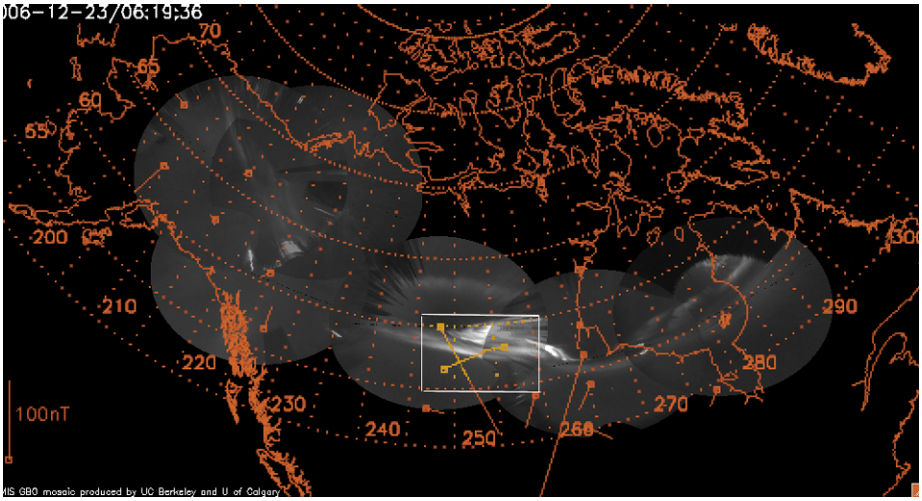

Fig. 7 Observations from the THEMIS ground-based observatories at 06:19:36 UT on December 23, 2006. The *white box* encompasses an auroral brightening accompanied by a strong shear in the directions of the magnetic field perturbations (red pointers extending from individual ground stations)

4.2 Macroscale Interactions

THEMIS will determine how the various localized, mesoscale substorm components interact over macroscale ranges for both the CD and Rx paradigms.

In the context of the CD paradigm, THEMIS will measure the velocity, magnetic, and plasma pressure perturbations associated with rarefaction waves propagating rapidly ($\sim$1600 km s^{-1}) antisunward at speeds comparable to the local fast mode speed (Chao et al. 1977). At onset, probes P3 and P4 should observe fast Earthward flows, followed by P2 some 20 s later. P1 will observe no Rx signature for at least another 20–25 s. The same THEMIS probes should track the outward motion of the rarefaction wave that links lobe flux dissipation to current disruption.

In the context of the Rx paradigm, THEMIS will track the sunward motion of the fast ($\sim$400 km s^{-1}) flows ejected from the reconnection region (Baumjohann et al. 1990; Angelopoulos et al. 1994). The anticipated delay time from P2 to P3 or P4 is greater than 90 s. In the second year, probe P5, separated in Z_{GSM} from the other inner probes, will determine if flow-driven boundary layer waves carry substantial Poynting flux. THEMIS probes P2, P3 and P4 will monitor the Earthward flow and establish the link between current disruption onset and reconnection.

Global MHD and particle codes will be used to model both specific events driven by measured solar wind parameters and idealized scenarios (Raeder et al. 2001, 2008). Particle modeling in prescribed E and B fields will validate the outgoing rarefaction wave or the incoming flow hypothesis (Li et al. 2000). Using MHD and particle simulations will strengthen closure on the macroscale interaction of components of the substorm instability.

By using the array of THEMIS spacecraft to determine the time and location of substorm onset, we have implicitly assumed that disturbances associated with substorms extend over a wide range of azimuths and propagate nearly radially towards or away from Earth. In fact, multipoint measurements in the magnetotail and on the ground indicate that the transient high-speed plasma flows that play such an important role in mass, energy, and magnetic flux

transport have spatial extents in the dawn-dusk direction limited to 2–5 R_E (Angelopoulos et al. 1997; Kauristie et al. 2000; Nakamura et al. 2004). By providing observations that map to a wide range of locations in the magnetotail, the dedicated array of THEMIS ground observatories will play a crucial role in selecting events with the wide azimuthal extents needed to ensure that all the THEMIS spacecraft observe the same phenomenon. In turn, with the help of appropriate magnetic field models, the ground observations can be used to determine the extent, and consequently the significance, of individual events.

4.3 Ionospheric Coupling

THEMIS will remotely infer (i) cross-tail current evolution and (ii) field-aligned current generation. By studying 100–200 substorms from various perspectives and local times relative to the onset meridian, THEMIS will establish the macroscale coupling between the global substorm instability and auroral arc formation.

During their second season in the magnetotail, THEMIS probes P4 and P5 will routinely straddle the current sheet at interspacecraft separations ranging from 0.2 to 1 R_E to measure the cross tail current strength (one to tens nA/m^2) and its evolution using a planar approximation. Tail flapping due to solar wind buffeting (Sergeev et al. 1998; Runov et al. 2005a, 2005b) and diurnal effects (Lopez 1990) ensure multiple neutral sheet crossings. Probe P2 observations will be used to determine the relationship between the current sheet motion and incoming flows.

When the inner THEMIS probes are away from the neutral sheet, they will obtain magnetic field measurements across and along the tail. The current disruption process can then be remotely sensed using methods established on ISEE-1/2 and Interball-1 observations (e.g., Jacquey 2000).

According to MHD theory, flow vorticity, flow braking, radial and cross-sheet pressure (p) gradients can generate field-aligned currents (Haerendel 1992; Shiokawa et al. 1998; Hesse and Birn 1991). Pairs of conjunctions between probes P4, P3, and P5 across the path of laterally expanding flow channels or tailward expanding pressure gradients will determine the vorticity and pressure gradients over scale sizes commensurate with the flow shear and expected pressure gradients. Observations by P2 further down the magnetotail will place the field-aligned currents within their global context.

The incoming flow interacts with the Earth's dipole in a region where there are strong gradients in the magnetic field strength and high ion temperatures. As a result, ion diamagnetic drifts are pronounced and non-MHD effects are readily apparent. Whereas ions gradient-curvature drift duskward, electrons follow $\mathbf{E} \times \mathbf{B}/B^2$ drifts. The distinction requires Hall MHD or hybrid simulations, and profoundly affects the generation of field-aligned currents (Yamade et al. 2000). In addition to plasma observations, electric field measurements become essential (Angelopoulos et al. 1999). THEMIS will measure both the plasma and $\mathbf{E} \times \mathbf{B}$ flows independently and will therefore determine the (non-MHD) component of the ion drifts.

Theory predicts current sheet structures with single-centered, single-off-centered, triple, and bifurcated current density peaks, limits on the minimum current sheet thickness, and the existence of flapping waves in the presence of anisotropic and non-gyrotropic plasmas (Sitnov et al. 2006). THEMIS observations of multiple current sheet crossings at different distances from the current sheet can be used to reconstruct the current sheet structure, including the identification of embedded flux rope structures, as a function of time or distance from the reconnection site (Nakamura et al. 2002, 2006; Runov et al. 2003, 2005b, 2006).

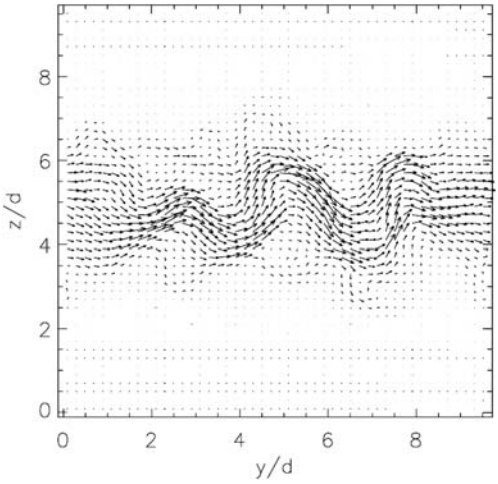

Fig. 8 A plot of the current density vectors in the plane perpendicular to the magnetotail axis from a full particle code simulation (Sitnov et al., 2006). Here d is the ion inertial scale length based on the density

During the second magnetotail season, the north-south displacement of spacecraft P5 relative to P3 and P4 will permit studies that track the thinning of the current sheet prior to substorm onset and the thickening that occurs thereafter.

Figure 8 presents model predictions for quasi-rectangular flapping waves superimposed upon the cross-tail current layer structure (Sitnov et al. 2006). When the spacecraft are azimuthally-separated, their observations can be used to determine the amplitude, wavelength, and propagation velocity and direction of these waves (Runov et al. 2005a). Similarly, azimuthal separations can be used to determine the characteristics of waves generated by ballooning-mode instabilities (Roux et al. 1991), thereby distinguishing between models invoking strong pressure gradients (Hurricane et al. 1999) and those based upon the velocity shears and the Kelvin-Helmholtz instability (Voronkov et al. 2000).

Finally, event-specific hybrid simulations will be used in conjunction with observations from probes P3, P4 & P5 to determine if observed CDs are due to electron acceleration accompanied by flux transport or a reduction in the ion drift rate.

4.4 Cross-scale coupling to local modes at 10 R_E

Substorms operate over a wide range of coupled scale-lengths (see Table 1). Identifying these coupling processes and determining when and where they occur is an essential aspect of substorm studies.

Ballooning modes Both geosynchronous (Roux et al. 1991) and ionospheric (Elphinstone et al. 1995) observations provide evidence for ballooning modes. Their free energy source is the pressure gradient in the near-Earth magnetotail (1 nPa R_E^{-1}). The modes have wavelengths ~2000–12000 km, move azimuthally at the 50–100 s km s^{-1} ion drift speed, and have Doppler-shifted periods of $T \sim 0.3$–2 min. Spacecraft traversing the near-Earth region at the $\sim 1\ R_E^2$ large onset location should observe coherent waves (Ohtani et al. 1993). Classical ballooning occurs near marginal stability for typical tail parameters (Lee and Wolf 1992; Hurricane et al. 1999). This has led to non-linear ballooning mode theories (Samson et al. 1996) and predictions for linear but absolute instabilities (Hurricane et al. 1999).

Shear-flow ballooning, an alternative approach, suggests that ballooning is part of a larger cross-scale coupling process (Voronkov et al. 1999, 2000). Field line resonances ($\lambda \sim 2$–$10\ R_E$, $T \sim 5$ min, e.g. Fenrich and Samson 1997) drive Kelvin-Helmholtz waves

Table 1 Scales of processes at substorm onset

Scale	Size (R_E)	Process
Macro	10	Rx/CD coupling. Current Wedge formation. Field line resonances
Meso	1	CD onset size. Ballooning modes. Kelvin-Helmholtz waves
Micro	0.1	Cross-field current instabilities. Alfvén waves

($\lambda \sim 0.2$–$1\ R_E$), which in turn become non-linearly unstable within ~1 min. The Kelvin-Helmholtz waves then drive smaller ($\delta Y \sim 0.1\ R_E$) Alfvénic currents that dissipate energy in the ionosphere. The azimuthal cross-field flow shear is on the order of $\delta V \sim 200\ \mathrm{km\,s^{-1}}$, while the waves have phase speeds $V_\phi \sim 50\ \mathrm{km\,s^{-1}}$. Independent Poynting vector calculations provide evidence for the bouncing Alfven waves (Maynard et al. 1996; Erickson et al. 2000), but their association with ballooning has not been confirmed.

During the second magnetotail season, azimuthal separations will enable probes P4 and P5 to study the coherent waves and resonances associated with ballooning modes using cross-spectral, wave-telescope (Motschmann et al. 1998) and Poynting vector techniques. Phase speeds calculated from observations by both probes at separations ranging from 0.3 to 10 R_E will be compared with flow speeds measured by each probe, and the properties of the waves will be compared with results from MHD simulations (e.g. Voronkov et al. 2000). Once again, simultaneous observations by probe P2 will provide the observations needed to determine the nature of coupling to the global substorm instability.

Cross-field current instabilities Cross-field current instabilities occur when the cross-tail current exceeds an instability threshold on the order of $10\ \mathrm{nA\,m^{-2}}$ or $100\ \mathrm{mA\,m^{-1}}$ (Lui 1996). They have frequencies of 0.01–$0.1\,f_{LH}$ (where the lower hybrid frequency $f_{LH} \sim 60$ Hz at $8\ R_E$), wavelengths on the order of 300–2000 km, and exhibit no cross-tail spectral coherence. Observations of the phase relationships between the electric and magnetic field observations will identify the mode and propagation direction of the unstable wave. Cross-tail probe pairs (P3, P4, P5) will determine the degree (if any) of spectral coherence. Particle-in-cell simulations (e.g., Büchner et al. 1998) will establish if the observed wave amplitudes and particle streaming compare favorably with non-linear saturation amplitudes of the unstable modes. P2 monitors coupling to the global substorm process.

4.5 Additional Tail Science

THEMIS can contribute towards understanding other important phenomena indirectly related to substorms. As these are not primary mission goals, they do not drive the mission design.

Ionospheric mapping Despite many years of research, establishing the relationship(s) between phenomena in the Earth's magnetotail and those in the high-latitude nightside auroral oval remains an important objective. Phenomena of interest in the ionosphere include flow channels, arcs, omega bands, and transpolar arcs, while those of interest in the magnetotail include bubbles, waves, and flux ropes. Azimuthal and latitudinal separations of the THEMIS spacecraft provide the gradients in velocity, pressure, and magnetic field strength and direction needed to calculate vorticity and field-aligned currents. These in turn can be mapped to the ionosphere and compared with auroral structures, and field-aligned currents

calculated from ground-based magnetometer and radar observations. Success in this endeavor would lead to the ability to routinely detect and understand substorm-related phenomena from ground-based observations alone.

Flux-tube evolution along streamlines Adiabatic convection cannot produce the observed average radial gradient in the lobe magnetic pressure, resulting in the so-called "pressure balance crisis" (Goertz and Baumjohann 1991; Erickson and Wolf 1980). Bubbles generated by uneven density loading in the magnetotail and propagating rapidly earthward have been proposed as the solution to this crisis (Pontius and Wolf 1990; Chen and Wolf 1993), but have only been observed during the late substorm phase (Sergeev et al. 1996). Working in conjunction with each other, THEMIS probes P4/P3, P2 and P1 will define the evolution of flux tubes as they move along streamlines, determine whether our ideas concerning bubble evolution are applicable to all flux tubes moving rapidly earthward, and provide an estimate of the importance of such bubbles in resolving the pressure balance crisis.

High frequency modes Waves in the Pi1 pulsation range (Perraut et al. 1998) or beyond (Shinohara et al. 1998) have been observed during substorms. They may be driven unstable by 0.5–2 keV electrons (Sugiyama et al. 1997) or free energy sources resulting from the kinetic structure of a thin plasma sheet (Le Contel et al. 1998). Bursty and broad-banded, they extend to $f \sim 4 f_{\mathrm{LH}}$ about 10–20% of the time. They are occasionally accompanied by whistlers at 1–10 f_{LH}. Burst waveform collection of **E** and **B** data at frequencies up to $10 \times f_{\mathrm{LH}}$ (or 600 Hz) will help identify their modes and place these waves in the context of substorm evolution.

5 Science Closure in the Outer Radiation Belt

Discriminating between the various source mechanisms for radiation belt particles requires equatorial measurements of radial phase space density profiles, particle spectra, and particle pitch angle distributions as a function of solar wind and geomagnetic conditions, including the occurrence patterns for both ULF and VLF waves. As illustrated in Fig. 9, in situ acceleration mechanisms generate local maxima in radial profiles for the phase space density, convective processes generate flat profiles, and diffusive processes generate positive radial gradients. Radial diffusion results in pitch angle distributions that peak perpendicular to the magnetic field, while wave-particle interactions keep particle distributions outside the loss cone nearly isotropic. Finally, flux enhancements propagate inward towards Earth from the point of injection, but both inward and outward from the point of energization.

Energetic particles drift in response to both transient and steady-state electric fields as well as in response to gradients in the magnetic field. Consequently, particle transport studies require comprehensive observations of the magnetospheric electric and magnetic field configuration, and the distribution of wave activity, as a function of geomagnetic and solar wind conditions. Proposed loss mechanisms are no less numerous than energization mechanisms. They include loss via scattering at the magnetopause or cross-tail current sheet and wave-particle scattering by resonant interaction with plasmaspheric hiss, whistler-mode chorus, and EMIC waves (Millan and Thorne 2007). Efforts to identify the principle loss mechanisms necessarily require accurate determination of particle drift paths to determine whether or not they intersect the current sheet or magnetopause, as well as information concerning the locations and intensity of plasma wave activity that can scatter particles into the loss cone and cause them to precipitate.

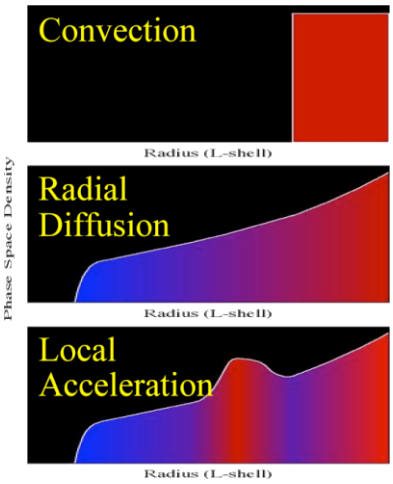

Fig. 9 Radial profiles of energetic particle phase space densities at constant first adiabatic invariant can be used as a tool to help distinguish between the various processes that energize particles within the Earth's radiation belts. In this figure *red shading* highlights potential source regions

The observed rapid increase of MeV electron flux inside of geosynchronous altitude cannot be accounted for by the relatively slow diffusion of solar wind plasma. The "Dst effect" alone cannot account for this process either, since the electrons first disappear and then reappear at much higher fluxes than before the storm. Electron fluxes are therefore likely enhanced at $L = 11$ before being transported inwards, but it is unclear if sufficient flux of electrons exists at such distances just prior to storm recovery.

The THEMIS probes traverse the inner magnetosphere from $L = 3.5$ to 11 with a median recurrence rate of 3.8 hours during their nominal phase (ranging from several up to 8 radial cuts per day). Thus, THEMIS will determine the radial profile of the electron phase space density at constant magnetic moment μ on time scales commensurate with the storm-time radiation belt MeV electron loss and re-appearance. Within the THEMIS mission, particle observations of the radiation belts are primarily the responsibility of the SST instrument. Although ESA can measure source populations at distances beyond geosynchronous orbit, penetrating radiation results in high background counts that dominate ESA measurements within the radiation belts.

Based on the slope of the obtained phase space density profiles versus L-shell, THEMIS will determine whether there is a sufficient source of electrons at the outer boundary. If the answer to this question is affirmative, THEMIS will identify the primary transport mechanism. The Dst-effect will be readily evaluated from individual radial flux profiles. The radial diffusion coefficient will be obtained from first order differencing of consecutive profiles, while the plasma convection will be directly measured on each probe. If radial transport alone cannot account for the MeV electron enhancement (Brautigam and Albert 2000), THEMIS, will determine whether other proposed mechanisms (e.g. in situ waves) are responsible for local electron heating.

As illustrated in Fig. 10, during the coast phase of the mission inter-spacecraft separation distances were on the order of 1–2 R_E within the radiation belts (radial distances from 2 to 6 R_E from Earth). Rapid consecutive visits by the different spacecraft to the same radial distance provide numerous opportunities to intercalibrate the particle instruments. Once the instruments were intercalibrated, the short separation distances enabled the calculation of radial gradients in the phase space density, a key discriminator between proposed particle energization mechanisms.

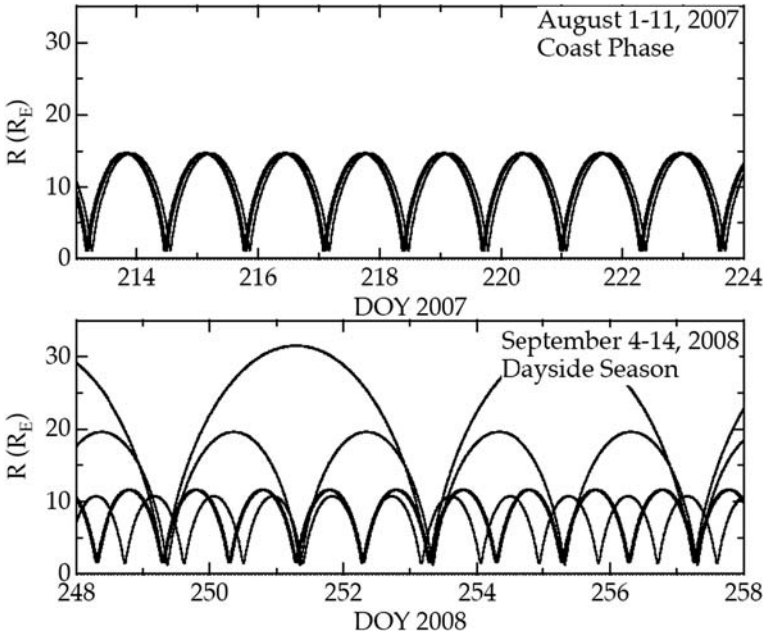

Fig. 10 The radial distances of the THEMIS spacecraft from Earth as a function of time during the coast phase and second dayside season

During later phases of the mission, illustrated in the lower panels of Fig. 10, separation distances of 1–2 R_E will remain common, but there will also be opportunities to compare energetic particle observations over the full range of radial distances from perigee to the 30 R_E apogee of the outermost spacecraft, P1. Large azimuthal and radial separation distances will enable researchers to track the motion of magnetic field dipolarizations and associated particle injection fronts, and determine whether processes other than adiabatic inward convection are needed to explain the particle populations seen near Earth (Fox et al. 2006).

Over the course of the mission, the THEMIS spacecraft will survey magnetospheric particle populations, electric and magnetic field configurations, and wave activity over the full range of local times for a wide range of solar wind and geomagnetic conditions. This information will be of critical importance in the development of new theoretical and empirical models for the Earth's radiation belts. Finally, THEMIS's ground observatories and its tail flow monitor P2 along with the radiation belt monitors P3, P4 and P5 promise to advance our knowledge of storm-substorm relationships.

6 Science Closure at the Dayside

6.1 Science Closure during the Baseline Dayside Mission

THEMIS's four probe conjunctions at the dayside recur once every 4 days and allow simultaneous measurements at the magnetopause, the foreshock and the pristine solar wind. Five-probe conjunctions recur once per 8 days, enabling simultaneous P3 and P4 measurements of the magnetopause with corresponding P5 measurements of the magnetosphere during the first dayside season, and simultaneous P3 and P4 measurements of the magnetopause with

corresponding P5 measurements of the magnetosheath in the second dayside season. As the P5's apogee moves outward by $\sim$1 R_E from the first to the second dayside season, the focus of attention for the three probes will move from the subsolar to the flank magnetopause. P1 serves as an upstream monitor in the pristine solar wind, P2 observes conditions within the foreshock, while P3 through P5 will determine the response of the magnetopause and magnetosphere.

These orbits offer an opportunity to identify solar wind or foreshock triggers for the full range of transient events observed at the bow shock, magnetopause, and in the outer dayside magnetosphere. Possible studies include determining the conditions under which hot flow anomalies or foreshock cavities attain large amplitudes (Sibeck et al. 2001), the impact of these upstream phenomena upon the magnetosphere and ionosphere, evidence for the initiation of reconnection at solar wind discontinuities transmitted into the magnetosheath (Phan et al. 2007), the search for southward IMF turnings (Lockwood and Wild 1993; Le et al. 1993) or solar wind/foreshock-generated pressure pulses (Potemra et al. 1992) as triggers of flux transfer events, as well as a determination of the predominant cause of magnetopause boundary motion (e.g. Borodkova et al. 1995).

Figure 11 presents global MHD model predictions for the interaction of an interplanetary shock with the Earth's magnetosphere (Samsonov et al. 2007). The figure shows profiles for the magnetic field strength, density, temperature, and velocity along the Earth-Sun line as a function of time. Following the arrival of the interplanetary shock, the bow shock (BS), magnetopause (MP), and a transmitted fast mode wave (FS) move Earthward. After the interval shown in the figure, the transmitted fast wave reflects from the plasmasphere/ionosphere, moves outward, and reverses the inward motion of the bow shock and magnetopause. At apogee, the innermost THEMIS spacecraft, indicated by asterisks in the bottom panel, are well situated to observe the motion of the bow shock and magnetopause. When deeper within the magnetosphere, the spacecraft will observe the passage of the transmitted and subsequent reflected fast mode waves as a set of well-defined correlated plasma and magnetic field perturbations.

6.2 Additional Science during the Coast Phase

The orbits of the 5 THEMIS spacecraft during the coast phase of the mission were ideal to study the structure of the magnetopause and bow shock, and the transients superimposed upon this structure. With a common apogee of 14.7 R_E, spacecraft apogees grazed the dusk magnetopause and the sub-solar bow shock. Separation distances ranging from 0.1 to 3 R_E permitted timing studies of flux transfer event, hot flow anomaly, and boundary wave motion along these boundaries, while similar separation distances perpendicular to the dayside magnetopause enabled researchers to measure the amplitude of boundary waves, test jump conditions, and determine how the layered structure of this boundary varies as a function of time and external conditions.

By definition, the magnetopause is a sharp ($\sim$600 km thick) boundary across which the magnetic field rotates from magnetosheath (shocked interplanetary) to magnetospheric magnetic field orientations. Past work suggests that the transition in plasma parameters is often far more gradual. A layer of magnetosheath plasma, known as the depletion layer, is often found immediately outside the magnetopause in the magnetosheath (Crooker et al. 1979). Similarly, there is often a low-latitude boundary layer of magnetosheath-like plasma on magnetospheric magnetic field lines just inside the magnetopause (Sckopke et al. 1981). The properties of these boundary layers are not well-known, but there are reasons to believe that the spatial extent and density variations associated with them become more pronounced during periods of strongly northward IMF orientation.

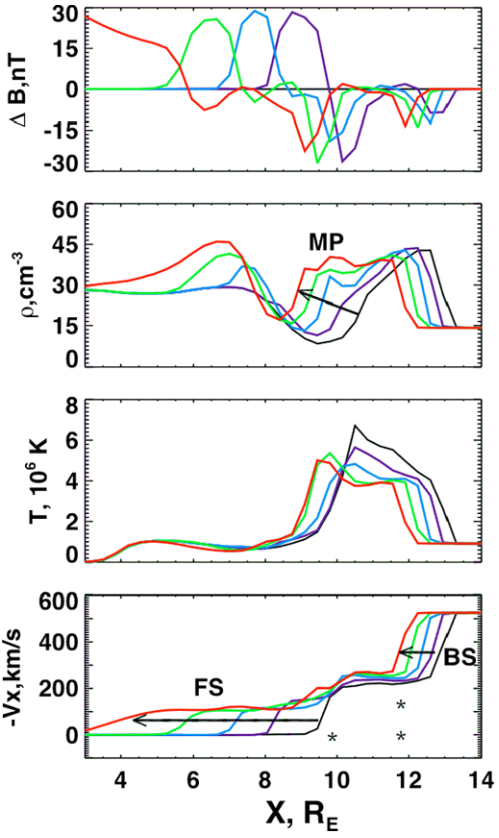

Fig. 11 Results from a global MHD simulation for the interaction of an interplanetary shock with the magnetosphere. The shock launches a transmitted fast mode wave (FS) that propagates through the magnetosheath and magnetosphere along the Earth-Sun line as a function of time (*black*, *blue*, *red* indicating successively later times during the simulation) (Samsonov et al. 2007). MP indicates the magnetopause, separating the low density magnetosphere from the high density magnetosheath. BS indicates the bow shock, separating superalfvénic flows in the solar wind from subAlfvénic flows in the magnetosheath. From *top* to *bottom*, the panels show the perturbation of the magnetic field strength, the density, the temperature, and the component of the velocity along the Earth-Sun line. Following their interaction with the transmitted waves, both the bow shock and magnetopause move inward towards the Earth. Stars in the *lower panel* indicate the apogees of THEMIS spacecraft P3–5 during the second dayside season

Several models have been proposed to account for the low-latitude boundary layer. During periods of southward IMF orientation, reconnection on the equatorial magnetopause should generate thin boundary layers on open magnetic field lines, marked by accelerated plasma flows and the loss of magnetospheric ions and electrons. During periods of northward IMF orientation, simultaneous reconnection at both cusps may append magnetosheath flux tubes with relatively uniform densities to the magnetosphere, resulting in sluggishly-moving boundary layers whose density varies little with radial distance. Diffusion should produce a boundary layer moving at speeds less than those in the nearby magnetosheath with a strong outward radial density gradient. The nonlinear Kelvin-Helmholtz instability should produce a complex structured boundary layer with rolled-up vortices of intermixed magnetosheath and magnetospheric plasma.

Figure 12 illustrates how the THEMIS spacecraft can be used to distinguish between these possibilities. When aligned nearly perpendicular to the nominal magnetopause, there will frequently be occasions when the spacecraft straddle the magnetopause, with two or more located within individual boundary layers. In this configuration, the spacecraft can be used to discriminate between boundary layers with near-uniform parameters, boundary layers exhibiting strong radial gradients, and boundary layers marked by complex local structures. Simultaneous magnetosheath, magnetospheric, and boundary layer observations can be used to compare boundary layer densities and velocities with predictions based on simultaneous magnetosheath and magnetospheric conditions.

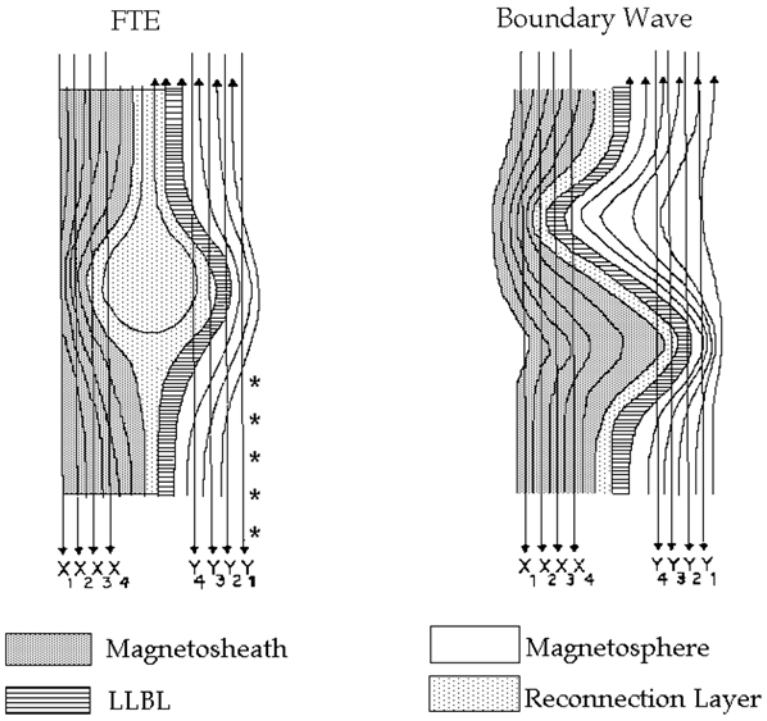

Fig. 12 A comparison of the FTE and pressure pulse models for transient events at the magnetopause (Lockwood 1991). Spacecraft at radially-separated locations in the magnetosheath and magnetosphere observe the events along the cuts labeled X1 to X4 and Y1 to Y4, respectively. Spacecraft arrayed parallel to the magnetopause (*asterisks*) can be used to time the motion and determine the velocity of the transient events

Transient structures, including both intrinsic Kelvin-Helmholtz and pressure-pulse driven boundary waves and flux transfer events (FTEs), are often superimposed upon the boundary layer structure. Whereas FTEs cause the magnetopause current layer to broaden and bulge outward simultaneously into both the magnetosheath and magnetosphere, boundary waves simply displace the magnetopause. Boundary waves driven by pressure pulses should be associated with pressure pulses in the magnetosheath, whereas those driven by the Kelvin-Helmholtz instability should not. Finally, FTEs should move with a velocity determined by the balance of pressure gradient and magnetic curvature forces, boundary waves driven by the Kelvin-Helmholtz instability should move antisunward in the direction of the magnetosheath flow, while those driven by pressure pulses should move in a direction determined by the orientation of the discontinuity associated with the pressure pulse sweeping across the magnetosphere.

As illustrated in Fig. 12, multipoint THEMIS observations will prove ideal in distinguishing between the predictions of these models for transient events. When arrayed perpendicular to the nominal magnetopause, the spacecraft can be used to distinguish between boundary waves and two-regime FTEs (Farrugia et al. 1987). Simultaneous observations of the magnetosheath and magnetosphere can be used to test whether conditions favor the occurrence of the Kelvin-Helmholtz instability during intervals when boundary waves are observed. When the spacecraft lie arrayed along the magnetopause (asterisks in Fig. 12), their observations can be used to determine FTE and boundary wave velocities, and whether they

move with the magnetosheath flow in a direction consistent with pressure pulses sweeping across the magnetosphere, or in a direction consistent with predictions for the interconnected magnetosheath and magnetospheric magnetic field lines expected within FTEs (Fear et al. 2007).

Many other topics regarding the detailed structure of the dayside magnetopause remain to be addressed. While four spacecraft can be used to determine the orientation, velocity, and thickness of discontinuities (Dunlop et al. 2002a, 2002b; Paschmann et al. 2005), observations by the five THEMIS spacecraft afford an opportunity to determine boundary acceleration and curvature. Furthermore, five spacecraft place greater constraints than four on efforts to recover boundary plasma and magnetic field structure via the Grad-Shafranov reconstruction technique (Walthour et al. 1993; Hasegawa et al. 2005). Finally, THEMIS observations may help researchers determine why boundary waves on the magnetotail flanks exhibit non-sinusoidal shapes that are inconsistent with the Kelvin-Helmholtz instability (Chen and Kivelson 1993).

7 Concluding Remarks

Substorms represent a fundamental mode of the solar wind-magnetosphere interaction, one involving a series of well-defined and repeatable steps leading to the abrupt release of solar wind energy stored within the Earth's magnetotail. Some of the energy is released into the Earth's ionosphere, some into the Earth's radiation belts, and some flows anti-sunward down the magnetotail. Despite their fundamental importance to magnetospheric physics, the absence of coordinated observations has long prevented a determination of the reasons for the sudden release of energy that occurs during substorms. In conjunction with theory and modeling, the array of ground- and space-based observations provided by THEMIS will offer an opportunity to pinpoint when and where this release occurs, precisely the information needed to understand the mechanisms driving substorms.

However, observations from THEMIS can be used to address a host of research problems in magnetospheric physics. These include the overall solar wind-magnetosphere interaction, as well as the mesoscale phenomena that occur within the foreshock and magnetosheath, reconnection, diffusion, and instabilities of the magnetopause, magnetosphere-ionosphere interactions, the characteristics of the aurorae and geomagnetic pulsations, and the processes that energize and remove particles in the Earth's radiation belts.

With its implementation of a complex mission involving multipoint ground- and space-based observations via a compact team, THEMIS will serve as a pathfinder for future NASA missions, including Magnetospheric Multiscale (MMS), Radiation Belt Storm Probes (RBSP), and Magnetospheric Constellation. The lessons learned from THEMIS, on topics ranging from multiple spacecraft and instrument builds, spacecraft commissioning and operations, through data analysis tools and open data systems, will be applied to these future missions. THEMIS inaugarates a new era in space research, one of cooperation and inclusiveness.

Acknowledgements Work at UCB and UCLA was supported by NASA Contract NAS5-02099. Work at NASA/GSFC was supported NASA's Explorer program and THEMIS MO&DA.

References

S.I. Akasofu, *Physics of Magnetospheric Substorms* (Reidel, Dordrecht, 1977)
V. Angelopoulos et al., J. Geophys. Res. **99**, 21257 (1994). doi:10.1029/94JA01263
V. Angelopoulos et al., J. Geophys. Res. **102**, 211 (1997). doi:10.1029/96JA03217
V. Angelopoulos et al., Geophys. Res. Lett. **18**, 2841 (1999). doi:10.1029/1999GL900601
V. Angelopoulos, Space Sci. Rev. (2008, this issue)
H. Auster et al., Space Sci. Rev. (2008, this issue)
D.N. Baker, T.I. Pulkinnen, V. Angelopoulos, W. Baumjohann, R.L. McPherron, J. Geophys. Res. **101**, 12975 (1996). doi:10.1029/95JA03753
D.N. Baker et al., Geophys. Res. Lett. **29** (2002). doi:10.1029/2002GL015539
W. Baumjohann et al., J. Geophys. Res. **95**, 3801 (1990)
T. Bösinger, K. Alanko, J. Kangas, H. Opgenoorth, W. Baumjohann, J. Atmos. Terr. Phys. **43**, 933 (1981)
J. Bonnell et al., Space Sci. Rev. (2008, this issue)
N.L. Borodkova, G.N. Zastenker, D.G. Sibeck, J. Geophys. Res. **100**, 5643 (1995)
D.H. Brautigam, J.M. Albert, J. Geophys. Res. **105**, 291 (2000)
J. Büchner et al., in *Geospace Mass and Energy Flow: Results from the ISTP Program*, ed. by A. Nishida, D.N. Baker, S.W.H. Cowley (AGU, Washington, 1998), p. 313
C. Carlson et al., Space Sci. Rev. (2008, this issue)
J.K. Chao et al., Planet. Space Sci. **25**, 703 (1977)
C.-X. Chen, R.A. Wolf, J. Geophys. Res. **98**, 21409 (1993)
S.-H. Chen, M.G. Kivelson, Geophys. Res. Lett. **20**, 2699 (1993)
C.R. Clauer, R.L. McPherron, J. Geophys. Res. **79**, 2811 (1974)
N.U. Crooker, T.E. Eastman, G.S. Stiles, J. Geophys. Res. **84**, 869 (1979)
P.W. Daly et al., Geophys. Res. Lett. **11**, 1070 (1984)
M.W. Dunlop, A. Balogh, K.-H. Glassmeier, J. Geophys. Res. **107** (2002a). doi:10.1029/2001JA005089
M.W. Dunlop, A. Balogh, K.-H. Glassmeier, P. Robert, J. Geophys. Res. **107** (2002b). doi:10.1029/2001JA005088
R.D. Elphinstone et al., J. Geophys. Res. **100**, 7937 (1995)
G.M. Erickson, R.A. Wolf, Geophys. Res. Lett. **7**, 897 (1980)
G.M. Erickson et al., J. Geophys. Res. **105**, 26265 (2000)
C.J. Farrugia, D.J. Southwood, S.W.H. Cowley, R.P. Rijnbeek, P.W. Daly, Planet. Space Sci. **35**, 737 (1987)
C.J. Farrugia, M.P. Freeman, S.W.H. Cowley, D.J. Southwood, M. Lockwood, A. Etamadi, Planet. Space Sci. **37**, 589 (1989)
R.C. Fear et al., Ann. Geophys. 1669 (2007)
F.R. Fenrich, J.C. Samson, J. Geophys. Res. **102**, 20031 (1997)
N.J. Fox, B.H. Mauk, J.B. Blake, Geophys. Res. Lett. **33** (2006). doi:10.1029/2006GL026598
H. Frey et al., Space Sci. Rev. (2008, this issue)
C.K. Goertz, W. Baumjohann, J. Geophys. Res. **96**, 20991 (1991)
J.C. Green, T.G. Onsager, T.P. O'Brien, D.N. Baker, J. Geophys. Res. **109** (2004). doi:10.1029/2004JA010579
G. Haerendel, in *ICS-1*, ed. by C. Mattock (European Space Agency, Noordwijk, 1992), p. 417
H. Hasegawa, B.U.Ö. Sonnerup, B. Klecker, G. Paschmann, M.W. Dunlop, H. Réme, Ann. Geophys. **23**, 973 (2005)
R.R. Heacock, J. Geophys. Res. **72**, 3905 (1967)
M. Hesse, J. Birn, J. Geophys. Res. **96**, 11513 (1991)
E.W. Hones Jr., in *Physics of Solar Planetary Environments*, ed. by D.J. Williams (AGU, Washington, 1976), p. 558
R.B. Horne, R.M. Thorne, S.A. Glauert, J.M. Albert, N.P. Meredith, R.R. Anderson, J. Geophys. Res. **100** (2005). doi:10.1029/2004JA010811
M.K. Hudson, A.D. Kotelnikov, X. Li, M. Temerin, J. Wygant, J.B. Blake, M.S. Gussenhoven, Geophys. Res. Lett. **22**, 291 (1995)
O.A. Hurricane, B.H. Fong, S.C. Cowley, F.V. Coroniti, C.F. Kennel, R. Pellat, J. Geophys. Res. **104**, 10221 (1999)
C. Jacquey, in *Magnetospheric Currents*, ed. by S.-I. Ohtani, R. Fujii, M. Hesse, R.L. Lysak (AGU, Washington, 2000), p. 275
K. Kauristie, V.A. Sergeev, M. Kubyshkina et al., J. Geophys. Res. **105**, 10677 (2000)
G. Kettmann, P.W. Daly, J. Geophys. Res. **93**, 7376 (1988)
G. Khazanov, M. Liemohn, T. Newman, M. Fok, A. Ridley, Ann. Geophys. **22**, 497 (2004)
B.T. Kress, M.K. Hudson, P.L. Slocum, Geophys. Res. Lett. **32** (2005). doi:10.1029/2005GL022373
M.V. Kubyshkina, J. Geophys. Res. **104**, 24977 (1999)

D. Larson et al., Space Sci. Rev. (2008, this issue)
G. Le, C.T. Russell, H. Kuo, Geophys. Res. Lett. **20**, 791 (1993)
O. Le Contel et al., in *ICS-4 Proceedings* (Kluwer Academic, Dordrech, 1998), p. 425
D.-Y. Lee, R.A. Wolf, J. Geophys. Res. **97**, 19251 (1992)
X. Li et al., Geophys. Res. Lett. **27**, 1447 (2000)
X. Li, D.N. Baker, S.G. Kanekal, M. Looper, M. Temerin, Geophys. Res. Lett. **28**, 3827 (2001)
K. Liou et al., J. Geophys. Res. **105**, 2495 (2000)
M. Lockwood, J. Geophys. Res. **96**, 5497 (1991)
M. Lockwood, M.N. Wild, J. Geophys. Res. **98**, 5935 (1993)
R.E. Lopez, Geophys. Res. Lett. **17**, 1671 (1990)
T.M. Loto'aniu, I.R. Mann, L.G. Ozeke, A.A. Chan, Z.C. Dent, D.K. Milling, J. Geophys. Res. **111** (2006). doi:10.1029/2005JA011355
A.T.Y. Lui, J. Geophys. Res. **101**, 13067 (1996)
A.T.Y. Lui et al., Geophys. Res. Lett. **7**, 721 (1988)
J. McFadden et al., Space Sci. Rev. (2008, this issue)
R.L. McPherron, T. Terasawa, A. Nishida, J. Geomagn. Geoelectr. **38**, 1089 (1986)
N.C. Maynard et al., J. Geophys. Res. **101**, 7705 (1996)
S. Mende et al., Space Sci. Rev. (2008, this issue)
R.M. Millan, R.M. Thorne, J. Atmos. Sol. Terr. Phys. (2007). doi:10.1016/j.jastp.2006.06.019
M.J. Mithaiwala, W. Horton, J. Geophys. Res. **110** (2005). doi:10.1029/2004JA010511
U. Motschmann et al., Multi-spacecraft filtering: Plasma mode recognition, in *Analysis Methods for Multi-Spacecraft Data* (Kluwer Academic, Dordrecht, 1998), p. 79
R. Nakamura et al., Geophys. Res. Lett. **29** (2002). doi:10.1029/2002GL016200
R. Nakamura et al., Geophys. Res. Lett. **31** (2004). doi:10.1029/2004GL019558
R. Nakamura et al., J. Geophys. Res. **111** (2006). doi:10.1029/2006JA011706
S.-I. Ohtani et al., J. Geophys. Res. **98**, 19355 (1993)
S.-I. Ohtani, J. Geophys. Res. **103**, 6815 (1998)
J.V. Olson, J. Geophys. Rev. **104**, 17499 (1999)
N. Omidi, D.G. Sibeck, J. Geophys. Res. **112** (2007). doi:10.1029/2006JA011663
A. Otto, D.H. Fairfield, J. Geophys. Res. **105**, 21175 (2000)
G.S. Paschmann et al., Ann. Geophys. **23**, 1481 (2005)
S.A. Perraut et al., in *ICS-4 Proceedings* (Kluwer Academic, Dordrecht, 1998), p. 349
A.A. Petrukovich et al., J. Geophys. Res. **103**, 47 (1998)
T.-D. Phan et al., Geophys. Res. Lett. **34** (2007). doi:10.1029/2007GL030343
D.H. Pontius, R.A. Wolf, Geophys. Res. Lett. **17**, 49 (1990)
T.A. Potemra, L.J. Zanetti, R. Elphinstone, J.S. Murphree, D.M. Klumpar, Geophys. Res. Lett. **19**, 1615 (1992)
J. Raeder et al., J. Geophys. Res. **106**, 381 (2001)
J. Raeder et al., Space Sci. Rev. (2008, this issue)
A. Roux et al., J. Geophys. Res. **96**, 17697 (1991)
A. Roux et al., Space Sci. Rev. (2008, this issue)
A. Runov et al., Ann. Geophys. **24**, 247 (2006)
A. Runov et al., Geophys. Res. Lett. **30**, 1579 (2003). doi:10.1029/2002GL016730
A. Runov et al., Ann. Geophys. **23**, 1391 (2005a)
A. Runov et al., Planet. Space Sci. **53**, 237 (2005b)
C.T. Russell, R.C. Elphic, Space Sci. Rev. **22**, 681 (1978)
J.C. Samson et al., in *ICS-3*, ed. by E.J. Rolfe, B. Kaldreich (European Space Agency, Noordwijk, 1996), p. 399
A.A. Samsonov, D.G. Sibeck, J. Imber, J. Geophys. Res. **112** (2007). doi:10.1029/2007JA01262
E.T. Sarris et al., Geophys. Res. Lett. **3**, 437 (1976)
N. Sckopke et al., J. Geophys. Res. **86**, 2099 (1981)
V.A. Sergeev, J. Geophys. Res. **101**, 2615 (1996)
V.A. Sergeev et al., J. Geophys. Res. **101**, 10817 (1996)
V. Sergeev et al., J. Geophys. Res. **103**, 9177 (1998)
I. Shinohara et al., J. Geophys. Res. **103**, 20365 (1998)
K. Shiokawa, W. Baumjohann, G. Haerendel, Geophys. Res. Lett. **24**, 1179 (1997)
K. Shiokawa, W. Baumjohann, G. Haerendel, Geophys. Res. Lett. **25**, 959 (1998)
D.G. Sibeck, R.B. Decker, D.G. Mitchell, A.J. Lazarus, R.P. Lepping, A. Szabo, J. Geophys. Res. **106**, 21675 (2001)
M.I. Sitnov, M. Swisdak, P.N. Guzdar, A. Runov, J. Geophys. Res. **111** (2006). doi:10.1029/2005JA011517
P. Song, R.C. Elphic, C.T. Russell, Geophys. Res. Lett. **15**, 744 (1988)

T. Sugiyama et al., Geophys. Res. Lett. **24**, 1651 (1997)
M.F. Thomsen, J.T. Gosling, S.J. Bame, K.B. Quest, C.T. Russell, J. Geophys. Res. **93**, 11311 (1988)
V.A. Troitskaya, J. Geophys. Res. **66**, 5 (1961)
A.Y. Ukhorskiy, B.J. Anderson, K. Takahashi, N.A. Tsyganenko, Geophys. Res. Lett. **33** (2006). doi:10.1029/2005GL024380
I. Voronkov et al., J. Geophys. Res. **104**, 17323 (1999)
I. Voronkov et al., J. Geophys. Res. **105**, 18505 (2000)
Y. Yamade et al., Geophys. Res. Lett. **27**, 1091 (2000)
D.W. Walthour et al., J. Geophys. Res. **98**, 1489 (1993)